Journal of African Earth Sciences 100 (2014) 524–531

Contents lists available at ScienceDirect

Journal of African Earth Sciences

journal homepage: www.elsevier.com/locate/jafrearsci

Stable-isotope stratigraphy of the Cenomanian–Turonian (Upper Cretaceous) boundary event (CTBE) in Wadi Qena, Eastern Desert, Egypt

Emad Nagm [a,b,*], Gamal El-Qot [c], Markus Wilmsen [d]

[a] Geology Department, Faculty of Science, Al-Azhar University, Assiut, Egypt[1]
[b] Geology Department, Faculty of Science, Taibah University, Saudi Arabia[2]
[c] Geology Department, Faculty of Science, Benha University, Benha, Egypt
[d] Senckenberg Naturhistorische Sammlungen Dresden, Museum für Mineralogie und Geologie, Sektion Paläozoologie, Königsbrücker Landstr. 159, D-01109 Dresden, Germany

ARTICLE INFO

Article history:
Received 18 April 2014
Received in revised form 30 July 2014
Accepted 31 July 2014
Available online 17 August 2014

Keywords:
Cenomanian–Turonian
CTBE
Chemostratigraphy
Eastern Desert
Egypt

ABSTRACT

A high-resolution $\delta^{13}C$ isotope record from Cenomanian–Turonian boundary interval of shallow marine successions in Egypt is presented. The $\delta^{13}C$ curves show the typical features of the globally documented Cenomanian–Turonian positive excursion, including three of the main positive isotope peaks defining the Cenomanian–Turonian Boundary Event (CTBE). Based on high-resolution ammonite biostratigraphy, the CTBE started in the study area above the Late Cenomanian *Neolobites vibrayeanus* Zone within the Galala Formation, directly above the global sequence boundary Cenomanian 5 (SB Ce 5). A stratigraphic gap at that level cuts out the lower a-peak of the CTBE. The Cenomanian–Turonian boundary is located within the upper part of the positive excursion between carbon excursion peaks c and d, coinciding with the boundary between the Late Cenomanian *Vascoceras cauvini* and the Early Turonian Vascoceratid zones. The CTBE ended up-section of peak d, at the base of the *Choffaticeras* spp. Zone. The amplitude of the positive $\delta^{13}C$ excursion in Egypt is very high (reaching 6.5‰ vs. V-PDB) and largely matches curves of European standard sections and others localities from different basins. Furthermore, the Lower Turonian Holywell Isotope Event, an important marker within the lowermost Turonian, has tentatively been recognized. The positive carbon stable isotope curves presented herein represent the outreach of the oceanic anoxic event (OAE) 2 in shallow-water nearshore sequences.

1. Introduction

The early Late Cretaceous Cenomanian–Turonian Boundary Event (CTBE) is one of the most important global Cretaceous positive carbon stable isotope events (e.g., Jarvis et al., 2006; Voigt et al., 2008; Wendler, 2013). This event occurred across the Cenomanian–Turonian boundary (about 93.9 Myr ago; Hinnov and Ogg in Gradstein et al., 2012) and reflects by one of the most extreme carbon cycle perturbations in Earth's history (oceanic anoxic event (OAE) 2, e.g., Sageman et al., 2006; Voigt et al., 2008; Jenkyns, 2010; Jarvis et al., 2011). Cretaceous OAEs, as originally defined by Schlanger and Jenkyns (1976) and Jenkyns (1980), were periods during which much of the world's oceans became severely depleted in oxygen and widespread deposition of organic carbon-rich sediments took place. Burial of organic carbon, which preferentially sequesters isotopically light carbon during OAEs, resulted in a positive $\delta^{13}C$ excursion in the geologic record and even if black shales are not developed, the carbon isotope excursions are useful markers for recognizing OAEs and facilitate trans-continental correlation (e.g., Gröcke et al., 1999; Takashima et al., 2006; Wendler et al., 2011). The positive carbon isotopic excursion accompanying OAE2 has been mainly been recorded from pelagic carbonate sediments (e.g., Jarvis et al., 2006, 2011; Voigt et al., 2007, 2008; van Bentum et al., 2009; Richardt and Wilmsen, 2012; Bomou et al., 2013), subordinately also from shallow marine successions (e.g., Elrick et al., 2009; Gertsch et al., 2010b; Wilmsen et al., 2010) and in terrestrial organic matter (e.g., Nemoto and Hasegawa, 2011). The importance of the less well studied nearshore OAE2 records, such as that of Egypt, is related to the fact that these settings are situated at the interface between open-ocean and terrestrial realms; such settings document important physical, biological, and climatic processes (e.g., sea-level changes) not readily detected in either pelagic or terrestrial deposits alone (Elrick et al., 2009). However, only a few studies (Gertsch et al., 2010a; El-Sabbagh et al., 2011; Anan et al., 2013) on Cenomanian–Turonian boundary nearshore successions in

* Corresponding author.
E-mail addresses: emad.nagm@yahoo.com (E. Nagm), g_elqot@yahoo.com (G. El-Qot), markus.wilmsen@senckenberg.de (M. Wilmsen).
[1] Permanent address.
[2] Current address.

http://dx.doi.org/10.1016/j.jafrearsci.2014.07.023
1464-343X/

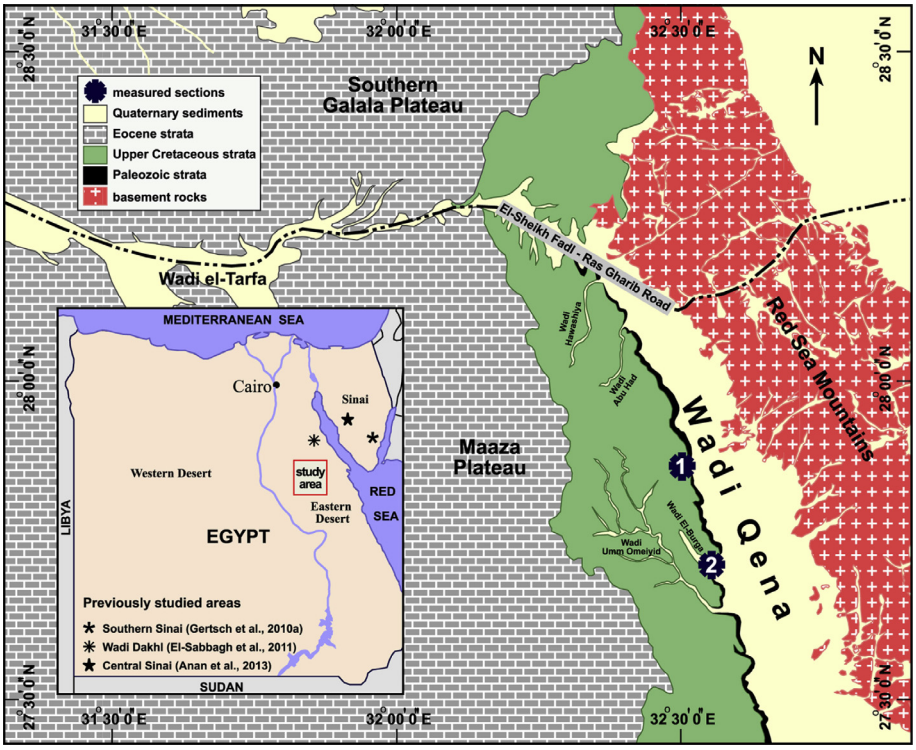

Fig. 1. Simplified geological map of the study area (modified after Conoco, 1987) with indication of the study area in Egypt and position of the measured Upper Cenomanian–Lower Turonian sections in Wadi Qena. Furthermore, the positions of sections where the CTBE isotope excursion has been studied in Egypt are provided.

Egypt have been conducted so far, leading to the identification of the CTBE excursion. The present paper aims at enhancing the knowledge about this important event by means of the stable isotopes ($\delta^{13}C$ and $\delta^{18}O$) records derived from well exposed sedimentary successions in Wadi Qena (Fig. 1), plotted against detailed litho-, bio- and sequence stratigraphic logs, providing a high-resolution stratigraphic reconstruction of the CTBE in Egypt. In addition, the $\delta^{13}C$ curve of the study area is correlated to the European CTBE reference section at Eastbourne, England, and to the Tethyan Pont d'Issole section, France, and to the Middle East Ghawr Al Mazar section, Jordan.

2. Geological setting

Marine Cenomanian–Turonian rocks are well-exposed in the northeastern part of Egypt in Sinai and the Eastern Desert. Wadi Qena occupies a large area in the northern and central parts of the Eastern Desert with well-exposed Upper Cretaceous successions at the western margin of the wadi (Fig. 1). From the southern slopes of the Southern Galala Plateau, Wadi Qena extends south-southeastwards for about 200 km down to the town of Qena where it grades into the River Nile valley. Wadi Qena is bordered by the serrated, varicoloured basement rocks of the Red Sea Mountains in the east and the uniform, elevated and flat-topped Maaza Plateau consisting of Eocene limestone in the west (Fig. 1).

Wadi Qena clearly developed along faults that run parallel to the Gulf of Suez and the Red Sea Mountains, which are well exposed at numerous places within the wadi, especially on the eastern side (Bandel et al., 1987). Most of the Paleozoic strata are non-marine and well-distributed in the northern part of the wadi. Marine transgression took place in the study area during early Late Cretaceous times when Egypt was situated at the southern margin of the Neotethys (Fig. 2). Following the Late Cenomanian transgression, the shoreline was located in southern part of Wadi Qena, indicated by strong siliciclastic input and the disappearance of marine strata to the south (e.g., Wilmsen and Nagm, 2013). The Cenomanian–Turonian ages witnessed the most widespread Cretaceous transgression in Egypt, with maximum flooding during Early Turonian times (e.g., Sharland et al., 2001; Wilmsen and Nagm, 2013). As a consequence, a widespread peri-continental shelf sea covered large parts of the area. The marine transgression continued (with some intermittent phases of regression) during the later parts of the Late Cretaceous and the Paleogene, documented by well-exposed and widely distributed Coniacian–Eocene strata as exposed in the western part of Wadi Qena (Fig. 1). The most recent sediments in the study area are the Quaternary alluvial fans which cover the low-lying plains of Wadi Qena (Fig. 1).

3. Sections and stratigraphic framework

Two sections from the central part of Wadi Qena in the north Eastern Desert have been measured in great detail at the western margin of the wadi. The mid-Wadi Qena section (no. 1 in Fig. 1) is located 30 km south of the El-Sheikh Fadl–Ras-Gharib road at 27°52′24″N and 32°32′48″E. The second section (Wadi El-Burga section, no. 2 in Fig. 1) is located 15 km south of mid-Wadi Qena section at the mouth of Wadi El-Burga entering Wadi Qena (27°45′12″N and 32°33′37″E). The succession starts with a non-marine sandstone unit (Naqus Formation) of Paleozoic age which consists of kaolinitic, white to yellowish-brown, well-sorted, medium to coarse-grained, cross-bedded sandstone with scattered quartz granules and pebbles. The top of the Naqus Formation contains intensive root traces that may indicate truncated paleosols, marking an erosional unconformity at the base of the overlying Galala Formation (Figs. 3 and 4). This surface has been equated with the late Middle Cenomanian sequence boundary Cenomanian 4 (SB Ce 4) that fused with the early Late Cenomanian transgressive surface of the following sequence (Wilmsen and Nagm, 2013).

The Galala Formation starts with silty, glauconitic sandstones yielding the trace fossil *Thalassinoides* isp. and fragmented mollusc

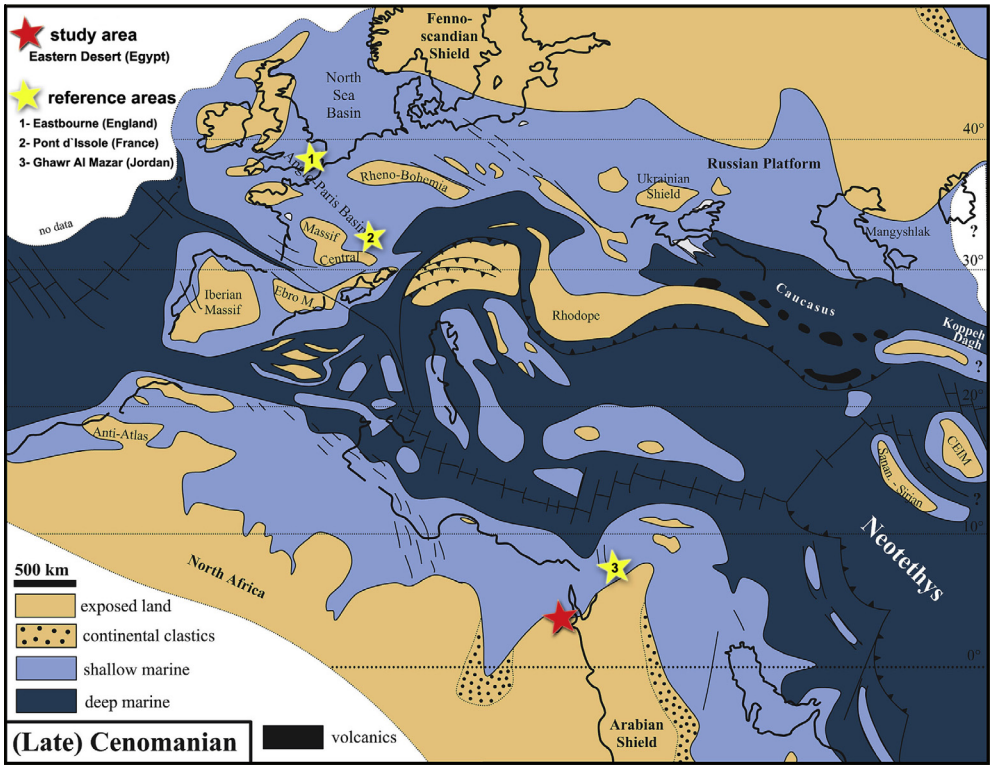

Fig. 2. Paleogeographic map of the Late Cenomanian, modified after Philip and Floquet (2000) with indication of the positions of study area and the reference sections used for chemostratigraphic correlations (see Fig. 5).

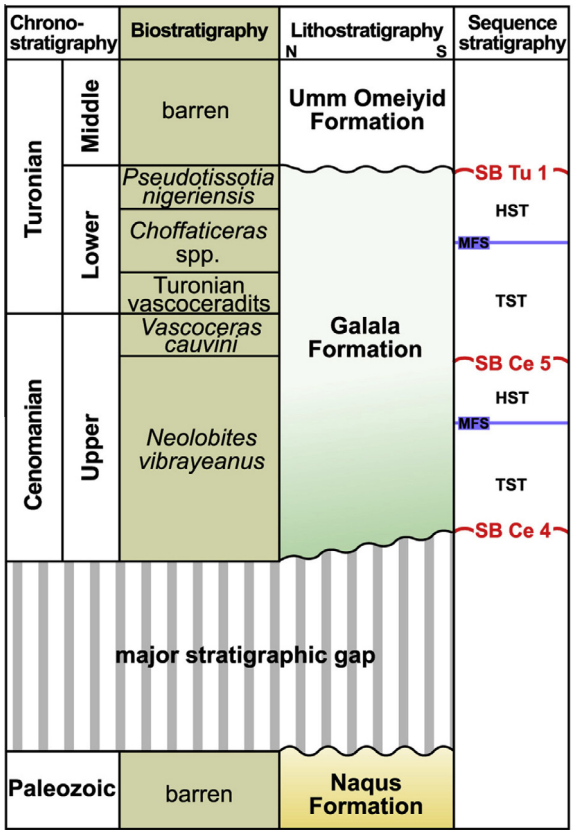

Fig. 3. Litho-, bio- and sequence stratigraphic framework of the study area (after Nagm and Wilmsen, 2012; Wilmsen and Nagm, 2013).

shells (mainly oysters), indicating shallow marine conditions. Shale beds are common up-section with few sandy limestones and thin bioturbated sandstone interbeds. The middle part of the Galala Formation consists of fossiliferous limestone bed. The following interval consists of gypsiferous shale grading into a highly fossiliferous limestone bed containing a typical lower Upper Cenomanian fauna (Nagm et al., 2011; Nagm and Wilmsen, 2012). This middle part of the Galala Formation is terminated by a sharp surface, representing an erosional unconformity that has been correlated with the mid-Late Cenomanian sequence boundary Cenomanian 5 (SB Ce 5; Wilmsen and Nagm, 2013). The upper part of the Galala Formation is very fossiliferous, containing abundant latest Cenomanian and Early Turonian ammonites (Nagm and Wilmsen, 2012). The Galala Formation is truncated along a prominent unconformity at the base of the Umm Omeiyid Formation, likewise marking the Lower–Middle Turonian boundary and representing the sequence boundary Turonian 1 (SB Tu 1, Fig. 3). According to Wilmsen and Nagm (2013), the three identified sequence boundaries (SB Ce 4 and 5, SB Tu 1) define two 3rd-order depositional sequences, each consisting of transgressive and highstand system tracts only. Falling stage and lowstand systems tracts are not developed due to a lack of accommodations space in this up-dip setting during falling and low sea-level (Wilmsen and Nagm, 2013).

The thickness of the Galala Formation is about 96 m at Mid-Wadi Qena section and reduced to 81 m at El-Burga section. Lithologically, the two sections are similar but in the southern part of the study area at El-Burga section, the lower part of the Galala Formation is more sandy while the middle and upper parts are less calcareous compared to the mid-Wadi Qena section at the north, containing more silt with thinner limestone beds (Fig. 4). These facies changes well reflect (along with the southward-reduced thicknesses) the distal (north) to proximal (south) gradients of the south Tethyan shelf in Egypt.

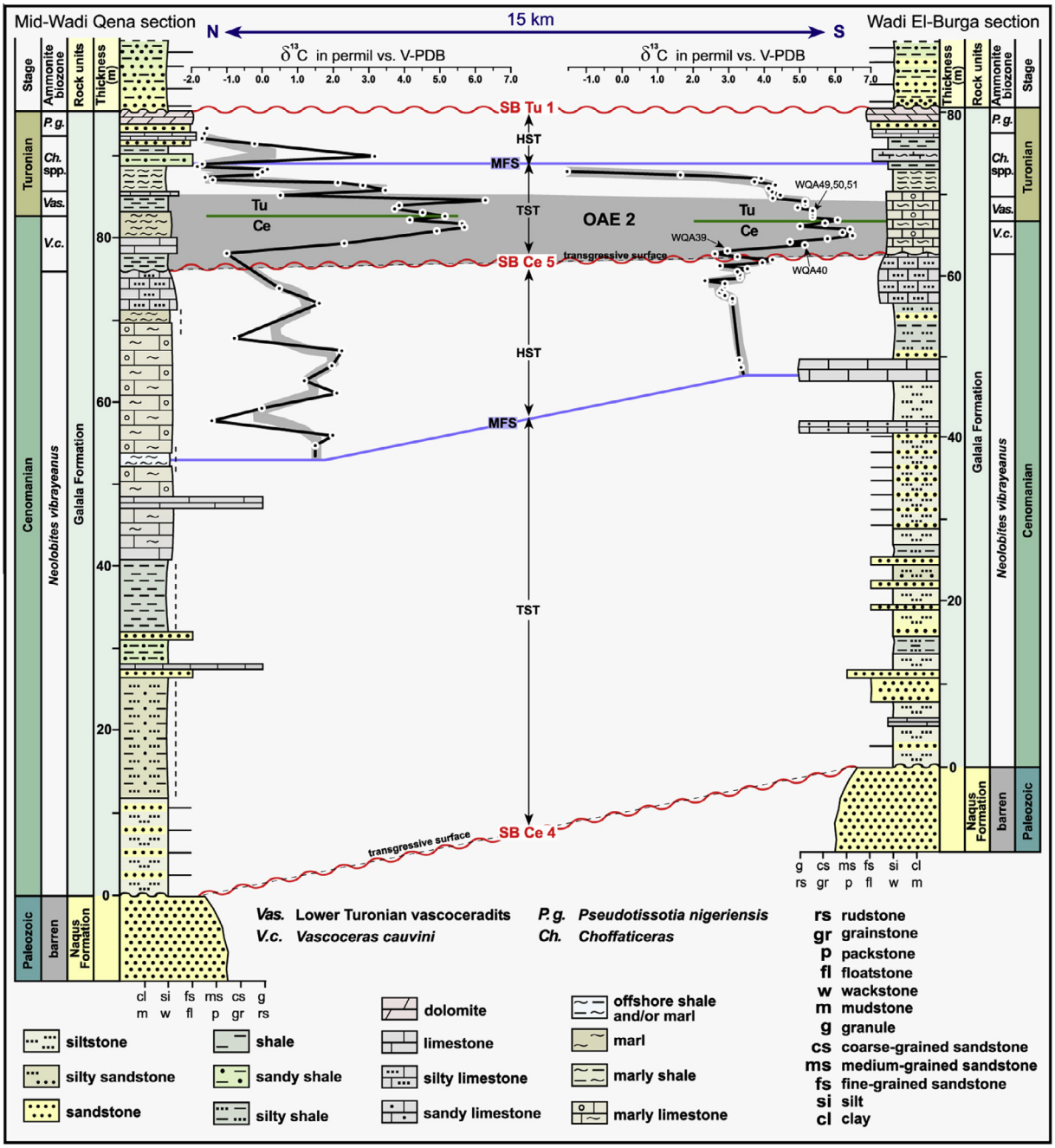

Fig. 4. Integrated stratigraphy (litho-, bio- and sequence stratigraphy) of the Upper Cenomanian–Lower Turonian in Wadi Qena, Eastern Desert supplemented with $\delta^{13}C$ curves.

Biostratigraphically, the Upper Cenomanian–Lower Turonian succession of the study area has been subdivided by means of high-resolution ammonite biostratigraphy (Figs. 3 and 4; cf. Nagm and Wilmsen, 2012). In the Upper Cenomanian, two zones have been recognized, i.e., a *Neolobites vibrayeanus* Zone at base (equivalent to the *Calycoceras naviculare* Zone) and *Vascoceras cauvini* Zone at the top (broadly equivalent to the *Neocardioceras juddii* Zone). Both zones are bounded at SB Ce 5. The gap between both zones in Wadi Qena comprises (most of) the mid-Upper Cenomanian *Metoicoceras geslinianum Zone* (Nagm et al., 2010a,b; Nagm and Wilmsen, 2012) and was interpreted as SB Ce 5 (Wilmsen and Nagm, 2013). The Early Turonian is represented by three ammonite zones, from base to top the Lower Turonian vascoceratids, *Choffaticeras* spp., and *Pseudotissotia nigeriensis* zones (Figs. 2–4; Nagm and Wilmsen, 2012), which have been correlated to the standard zones of *Watinoceras coloradoense* and *Mammites nodosoides* (Nagm and Wilmsen, 2012).

4. Stable-isotope stratigraphy

4.1. Methods

In total 102 samples were collected from the Upper Cenomanian–Lower Turonian strata of the sections for stable isotope analyses ($\delta^{13}C$ and $\delta^{18}O$), every ~40 cm at Wadi El-Burga and every ~75 cm at Mid-Wadi Qena section (Fig. 4, Table 1). A carbonate powder has been produced from each collected rock sample by

using a microdrill and was filled into lab-specific containers that enter the analytical line. In the isotope lab of GeoZentrum Nordbayern (Erlangen), the carbonate powders have been reacted with 100% phosphoric acid at 70 °C using a Gasbench II connected to a ThermoFinnigan Five Plus mass spectrometer. All values are reported in permil relative to V-PDB by assigning a $\delta^{13}C$ value of +1.95‰ and a $\delta^{18}O$ value of −2.20‰ to NBS19. Reproducibility was checked by replicate analyses of the laboratory standards and was better than ±0.08 for $\delta^{13}C$ and ±0.09 for $\delta^{18}O$. In the mid-Wadi Qena section, $\delta^{13}C$ values vary between −8.68‰ and 6.36‰ (mean 1.06‰) and $\delta^{18}O$ values vary between −9.61‰ and −0.65‰ (mean −6.23‰). In the Wadi El Burga section, $\delta^{13}C$ values vary between −1.97‰ and 6.44‰ (mean 3.54‰) and $\delta^{18}O$ values vary between −9.48‰ and −3.83‰ (mean −5.67‰). $\delta^{18}O/\delta^{13}C$ crossplots show no significant correlation (mid-Wadi Qena section: $R^2 = 0.37$; Wadi El Burga section: $R^2 = 0.23$).

4.2. Carbon stable isotopes ($\delta^{13}C$)

The $\delta^{13}C$ values of the lower Upper Cenomanian *N. vibrayeanus* Zone are low in both sections, scattering around zero in the mid-Wadi Qena section and around 1.0‰ at Wadi El Burga (Fig. 4). In the latter section, there is a trend to increased values in the upper part of the zone of up to ca. 3.0‰. Above the level of SB Ce 5, a distinct and abrupt increase in isotope values is evident from both sections. In the Cenomanian–Turonian boundary interval (from the base of *Vascoceras cauvini* Zone, SB Ce 5, to the level of the Lower Turonian *Choffaticeras* Zone), $\delta^{13}C$ values are high, forming a significant positive carbon isotope excursion (CIE), and reaching maximum values of up to 6.44‰. There are three distinct peaks of $\delta^{13}C$ values in the positive CIE, a lower one in the middle part of the *Vascoceras cauvini* Zone, a middle one in the upper part of the same zone, and a upper one located low in the lowermost Turonian Vascoceratid Zone (Fig. 4). Above this upper maximum, $\delta^{13}C$ values generally decrease with some subordinate small-scale peaks in the Lower Turonian to values that prevailed below SB Ce 5, forming a minimum within the mid-Lower Turonian *Choffaticeras* spp. Zone (Fig. 4).

4.3. Oxygen stable isotopes ($\delta^{18}O$)

The $\delta^{18}O$ values range from −9.61‰ to −0.65‰ (Table 1). These in part very low values may indicate considerably changes during burial diagenesis with a corresponding depletion of $\delta^{18}O$ values. Therefore, we do not use them neither for correlation purposes nor for palaeo-temperature reconstructions. However, the poor correlation of $\delta^{18}O$ and $\delta^{13}C$ argues for a selective diagenetic overprint only of the oxygen isotope values while the diagenetically more stable $\delta^{13}C$ values appear to reflect a predominantly pristine signal.

Table 1
Isotope values ($\delta^{13}C$ and $\delta^{18}O$) of the Upper Cenomanian–Lower Turonian in the two studied sections.

Mid-Wadi Qena section			Wadi El-Burga section		
Sample	d13C	d18O	Sample	d13C	d18O
Lower Turonian			*Lower Turonian*		
WQB 58	−0.72	−4.71	WQA 66	−1.42	−9.48
WQB 57	−1.21	−5.40	WQA 65	0.10	−4.30
WQB 56	−1.78	−5.98	WQA 64	0.07	−4.44
WQB 55	−2.07	−6.18	WQA 63	−1.97	−4.50
WQB 54	−0.28	−4.12	WQA 62	1.68	−5.15
WQB-53	3.23	−0.65	WQA 61	3.90	−5.19
WQB-52	−8.68	−8.44	WQA 60	3.78	−6.42
WQB 51	−6.74	−7.57	WQA 59	4.33	−4.49
WQB 50	0.27	−4.77	WQA 58	4.09	−5.34
WQB 49	0.07	−5.61	WQA 57	4.29	−4.56
WQB 48	−0.06	−5.24	WQA 56	4.44	−6.19
WQB 47	−1.62	−0.72	WQA 55	4.28	−6.96
WQB 45	−0.35	−3.41	WQA 54	5.14	−4.03
WQB 44	2.18	−4.44	WQA 53	5.11	−4.86
WQB 43	2.98	−4.96	WQA 52	4.98	−5.48
WQB 42	3.51	−4.49	WQA 51	5.32	−4.60
WQB 41	0.49	−5.85	WQA 50	5.33	−5.29
WQB 40	6.36	−4.36	WQA 49	5.30	−5.00
WQB 39	4.20	−5.44	WQA 48	6.09	−5.81
WQB 38	4.34	−5.39			
WQB 37	4.55	−5.82	*Upper Cenomanian*		
WQB 36	5.14	−5.27	WQA 47	5.83	−5.80
			WQA 46	5.00	−5.93
Upper Cenomanian			WQA 45	6.41	−4.99
WQB 35	4.23	−5.46	WQA 44	6.21	−5.83
WQB 34	5.68	−4.80	WQA 43	6.44	−5.49
WQB 33	5.73	−4.75	WQA 42	5.73	−4.93
WQB 32	4.95	−4.48	WQA 41	4.76	−3.83
WQB 31	2.39	−6.19	WQA 40	5.15	−4.59
WQB 30	−1.05	−9.30	WQA 39	2.97	−6.96
WQB 29	0.51	−8.98	WQA 38	2.60	−8.16
WQB 28	1.67	−7.45	WQA 37	3.29	−6.94
WQB 27	0.84	−8.37	WQA 36	4.26	−4.82
WQB 26	2.22	−7.59	WQA 35	3.90	−6.86
WQB 25	2.05	−6.60	WQA 34	2.75	−7.64
WQB 24	1.26	−7.98	WQA 33	3.59	−6.12
WQB 23	2.12	−7.02	WQA 32	3.26	−4.91
WQB 22	0.06	−8.17	WQA 31	3.32	−5.61
WQB 21	−1.64	−9.61	WQA 30	3.33	−5.00
WQB 20	2.06	−6.95	WQA 29	2.34	−8.94
WQB 19	1.54	−7.48	WQA 28	2.87	−6.72
WQB 18	2.07	−7.26	WQA 27	2.83	−7.43
WQB 17	1.63	−7.38	WQA 26	2.86	−6.83
WQB 16s	−1.50	−6.95	WQA 25	2.74	−5.17
WQB 16	−1.26	−9.38	WQA 24	2.89	−5.36
WQB 15	−0.18	−8.82	WQA 23	3.14	−4.91
WQB 14	1.71	−7.21	WQA 22	3.12	−4.50
WQB 13	1.81	−6.62	WQA 20	3.32	−5.55
WQB 12	−2.81	−9.21	WQA 19	3.40	−4.61
WQB 9s	−1.24	−4.39	WQA 18	3.22	−5.61
WQB 9	−2.22	−7.68	WQA 17	0.62	−4.57
WQB 8	−1.49	−9.10	WQA16	0.08	−6.57
WQB 6	−1.94	−7.23	WQA 14	−1.48	−8.02

5. Discussion and conclusions

The well-known positive $\delta^{13}C$ excursion spanning the Cenomanian–Turonian boundary is one of the main carbon isotope events in the geologic record and represents one of the largest perturbations of the global carbon cycle during the last 110 Myr (Jenkyns, 1980; Schlanger et al., 1987; Jarvis et al., 1988, 2006, 2011; Paul et al., 1999; Tsikos et al., 2004; Sageman et al., 2006; Voigt et al., 2007, 2008; Wendler et al., 2011; Wendler, 2013). It has predominantly been recorded from open-marine successions because of their potentially more complete stratigraphic record and the potentially strong diagenetic overprint of $\delta^{13}C$ records in shallow-water sections (e.g., Gertsch et al., 2010b). Good quality records from nearshore settings are thus comparably rare (e.g., Hilbrecht et al., 1996; Voigt et al., 2006; Wilmsen et al., 2010). Furthermore, organic-rich sediments (e.g. black shales) as sedimentary markers of ocean anoxia are rare or lacking in sections from inner ramp and coastal environments (Van Buchem et al., 2002; Lüning et al., 2004). Thus, additional $\delta^{13}C$ records from shallow-water successions may help to shed light on the conditions that dominated during oceanic anoxic event (OAE) 2.

In Egypt, sections from Sinai (Wadi El-Ghaib: Gertsch et al., 2010a; Wadi Feiran: El-Sabbagh et al., 2011; Gabal Musabaa Salama, Gabal Ekma and Gabal Qabaliate: Anan et al., 2013) and one section from the Eastern Desert (Wadi Dakhl: El-Sabbagh et al., 2011) have been studied for the presence of the positive carbon isotope excursion of the OAE2. In all these sections, the $\delta^{13}C$ records reach up to 5‰ vs. V-PDB, indicating the presence of the

event, but the main peaks which subdivide the positive OAE2 carbon isotope excursion (CIE) into distinct segments (see below) are poorly resolved. Taking into account the strong syn- and post-depositional tectonic activity in Sinai and the north Eastern Desert related to the structural system of the Syrian Arc (Said, 1990; Kuss et al., 2000; Rosenthal et al., 2000), the relatively poor $\delta^{13}C$ signals of the mentioned sections are interpreted here as a result of strong tectonically induced diagenetic overprint. In contrast, the Wadi Qena sections studied herein are situated on the stable part of the southern Tethyan shelf and are thus less prone to diagenetic alteration (another section situated in Wadi Araba in the northern part of the Eastern Desert yielded strongly depleted $\delta^{13}C$ values, giving support for our interpretation). Furthermore, the Wadi Qena sections are subdivided by means of high-resolution ammonite biostratigraphy (Nagm and Wilmsen, 2012) which is lacking for most of the other mentioned sections.

The stable isotope analysis of the Upper Cenomanian–Lower Turonian Galala Formation of Wadi Qena resulted in a $\delta^{13}C$ curve that clearly displays the positive CIE of the OAE2 (Fig. 4). The $\delta^{13}C$ values are fairly high (reaching up to 6.44‰) in comparison to south Tethyan (e.g. Jordan Ghawr Al Mazar section; Wendler et al., 2014) and north Tethyan (e.g. Pont d'Issole, France; Jarvis et al., 2011) as well as northwest European epicontinental sections (e.g., Eastbourne, England; Paul et al., 1999; Jarvis et al., 2006), but the amplitude of the positive excursion is very similar (positive shift of 3.5–4.5‰ $\delta^{13}C$). The new $\delta^{13}C$ data (Fig. 5) also record most of the typical features of the positive OAE 2 CIE that has been subdivided into segments based on a number of superimposed peaks (Paul et al., 1999; Sageman et al., 2006; Jarvis et al., 2006, 2011; Voigt et al., 2007, 2008). Herein, we follow the approach of Voigt et al. (2007, 2008) who recognized four peaks (a–d) within the OAE 2 CIE of which the a- to c-peaks characterize the latest Cenomanian part while the d-peak is an earliest Turonian feature. Rising and/or falling segments as well as plateaus characterize the inter-peak intervals of the curve. The temporal framework of the OAE 2 CIE is well known: it started ca. 400 kyr before the Cenomanian–Turonian boundary at 93.9 Ma (Ogg and Hinnov in Gradstein et al., 2012) and ranges just into the Early Turonian, thus lasting 400–500 kyr (Sageman et al., 2006; Voigt et al., 2008). The base of the *M. nodosoides* Zone is at ca. 93.5 Ma.

In contrast to the reference curves at Eastbourne and Pont d'Issole, there are only two Late Cenomanian peaks in the Wadi Qena curve (Fig. 5), the lower one in the middle part of the *V. cauvini* Zone and the upper one very close to the biostratigraphically defined Cenomanian–Turonian boundary. The abrupt increase of $\delta^{13}C$ values above the level of sequence boundary SB Ce 5 in Wadi Qena from around 3‰ to the lower conspicuous maximum of ~6.5‰ can be correlated to the rising segment between the a- and b-peaks of the European standard curve, the maximum corresponding to the b-peak (Fig. 5). This means that the rising segment and the a-peak of the lower and middle *M. geslinianum* Zone fall into a stratigraphic gap at Wadi Qena. This gap has biostratigraphically been demonstrated by Nagm and Wilmsen (2012) and genetically been explained by Wilmsen and Nagm (2013) by a major sea-level fall, lowstand and subsequent rise (onlap onto the subaerial unconformity) at SB Ce 5 in Wadi Qena. This unconformity can be traced across the Eastern Desert of Egypt (Wilmsen and Nagm, 2013) and can safely be correlated to the sub-*plenus* erosion surface at Eastbourne (Paul et al., 1999), a marked facies change at the base of the Niveau Thomel at Pont d'Issole (Jarvis et al., 2011), and probably to a sequence boundary (CeJo4) in the uppermost Hummar Formation at Ghawr Al Mazar, Jordan (Wendler et al., 2014). The correlation also shows that the *N. vibrayeanus* Zone underlying SB Ce 5 at Wadi Qena is temporally equivalent to the *C. guerangeri* Zone in Europe (as biostratigraphically proposed by Nagm et al., 2010a,b). Furthermore, the lower part of the Egyptian

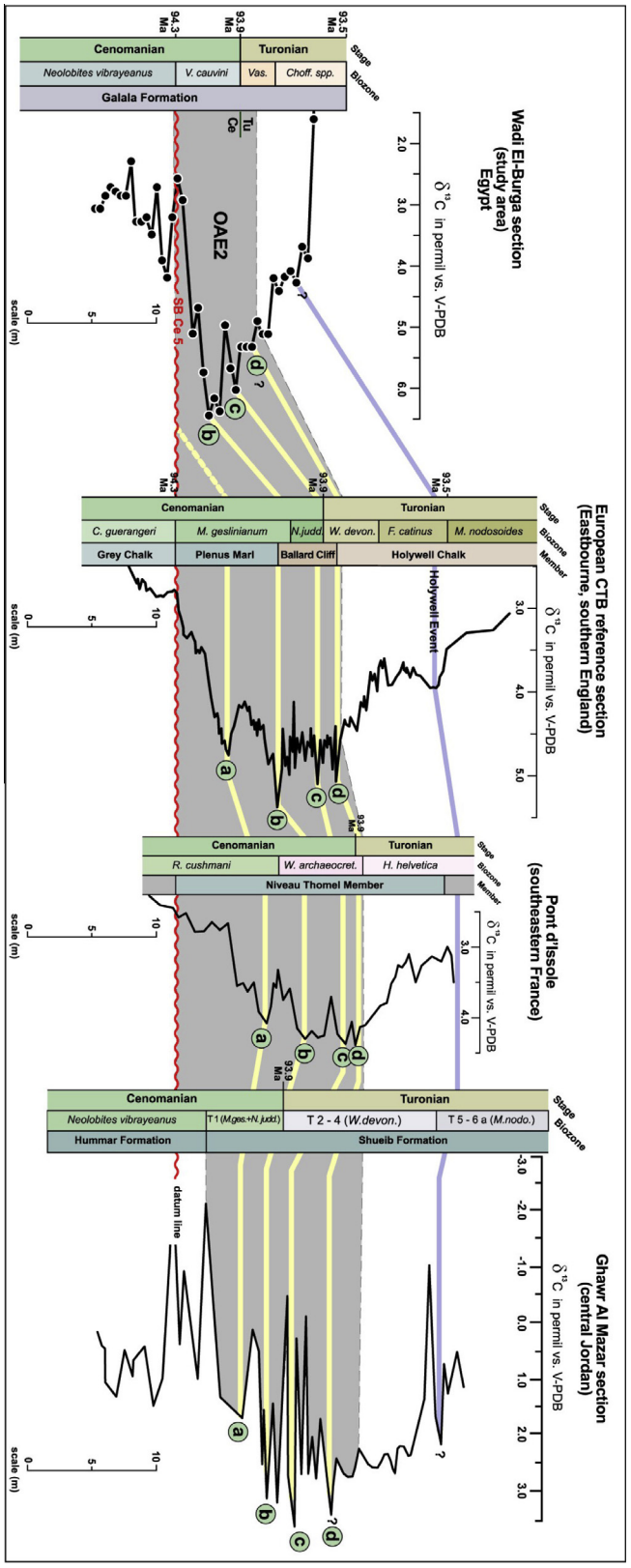

Fig. 5. $\delta^{13}C$ curve of the Cenomanian–Turonian boundary interval of Wadi Qena (left, this study) correlated to the European OAE 2 reference section at Eastbourne (Paul et al., 1999), the Tethyan Pont d'Issole section, France, at the northern Tethyan margin (Jarvis et al., 2011), and the Ghawr Al Mazar section (central Jordan) at the southern Tethyan margin (Wendler et al., 2014). Position of Holywell Event in Ghawr Al Mazar section after Wendler et al., 2010. The main peaks of the positive $\delta^{13}C$ excursion defining the OAE 2 are indicated. Time scale after Gradstein et al. (2012).

V. cauvini Zone (containing the b-peak) is equivalent to the upper part of the *M. geslinianum* Zone and only their upper part corresponds to the European *N. juddii* standard zone. This result specifies the interpretation of a temporal concordance of the *V. cauvini* and *N. juddii* zones (Nagm et al., 2010b).

The second peak of the Wadi Qena curve is very close to the biostratigraphically defined Cenomanian–Turonian boundary (base of Turonian vascoceratids) and corresponds to the c-peak of the OAE 2 CIE (Fig. 5). In the expanded CTB reference section of Eastbourne, the boundary is placed immediately above this peak (Paul et al., 1999; Jarvis et al., 2006; Voigt et al., 2008), thus demonstrating the correspondence of bio- and chemostratigraphic interpretations. The earliest Turonian d-peak usually attains a similar magnitude as the c-peak in most sections and is thus only provisionally placed in the Wadi Qena curve where it is less pronounced (Fig. 5). It may be that parts of this interval of the Wadi Qena curve are affected by a minor hiatus in the Cenomanian–Turonian boundary interval that has biostratigraphically been recognized in sections from Wadi Araba in the northern part of the Eastern Desert (see Nagm et al., 2010b).

The Early Turonian segment of the Wadi Qena curve displays the characteristic stepwise decrease to pre-OAE 2 $\delta^{13}C$ values (Fig. 5), known from isotope curves across the globe (see Jarvis et al., 2006 and Wendler, 2013 for compilations). A minor change in the gradient of this falling limb punctuated by a small peak may be correlated to the Holywell Event of Jarvis et al. (2006). The onset of this plateau-like segment of the curve matches the base of the *Choffaticeras* spp. Zone in the biozonation of the Eastern Desert (Nagm et al., 2010a,b; Nagm and Wilmsen, 2012). Calibrated to the Eastbourne curve, this correlation suggests that this level corresponds to the base of the *F. catinus* Zone in England.

In conclusion, the herein presented case study provides an ostensive example of the success of integrated stratigraphic approaches, combining bio-, sequence and chemostratigraphy, for high-resolution correlations across different tectonic plates. Furthermore, it highlights the potential of carbon stable isotope stratigraphy also for the dating of shallow-water successions and the calibration of biozonations in different palaeo-biogeographical realms.

Acknowledgements

Jochen Kuss (Bremen University, Germany) and an anonymous reviewer made valuable and constructive suggestions to improve the manuscript. Many thanks to Patrick Eriksson (University of Pretoria, South Africa) for editorial work. Financial support by the German Research Foundation (DFG) to MW (Project Wi 1743/6-1 and / 6-2) is gratefully acknowledged. We also thank B. Niebuhr and N. Janetschke (MMG-SNSD, Dresden), Marouf Abdelhamid (Ain Shams University, Egypt) and Adel Afify (Benha University, Egypt) for help during fieldwork.

References

Anan, T.I., El-Shahat, A., Genedi, A., Grammer, M., 2013. Depositional environments and sequence architecture of the Raha and Abu Qada formations (Cenomanian–Turonian), west central Sinai, Egypt. J. Afr. Earth Sci. 82, 54–69.

Bandel, K., Kuss, J., Malchus, N., 1987. The sediments of Wadi Qena (Eastern Desert, Egypt). J. Afr. Earth Sci. 6 (4), 427–455.

Bomou, B., Adatte, T., Tantawy, A., Mort, H., Fleitmann, D., Huang, Y., Föllmi, K.B., 2013. The expression of the Cenomanian–Turonian oceanic event in Tibet. Palaeogeogr. Palaeoclimatol. Palaeoecol. 369 (2013), 466–481.

Conoco, C., 1987. Geological Map of Egypt. The Egyptian General Petroleum Corporation, Cairo.

Elrick, M., Molina-Garza, M., Duncan, R., Snow, L., 2009. C-isotope stratigraphy and paleoenvironmental changes across OAE2 (mid-Cretaceous) from shallow-water platform carbonates of southern Mexico. Earth Planet. Sci. Lett. 277, 295–306.

El-Sabbagh, A., Tantawy, A., Keller, G., Khozyem, H., Spangenberg, J., Adatte, T., Gertsch, B., 2011. Stratigraphy of the Cenomanian–Turonian oceanic anoxic event OAE2 in shallow shelf sequences of NE Egypt. Cretac. Res. 32 (6), 705–722.

Gertsch, B., Keller, G., Adatte, T., Berner, Z., Kassab, A.S., Tantawy, A.A., El-Sabbagh, Stueben, D., 2010a. Cenomanian–Turonian transition in a shallow water sequence of the Sinai∗ Egypt. International Journal of Earth Sciences 99 (1), 165–182.

Gertsch, B., Adatte, T., Keller, G., Tantawy, A.A., Berner, Z., Mort, H., Fleitmann, D., 2010b. Middle and late Cenomanian oceanic anoxic events in shallow and deeper shelf environments of western Morocco. Sedimentology 57 (6), 1430–1462.

Gradstein, F.M., Ogg, J.G., Hilgen, F.J., 2012. On the geologic time scale. Newsl. Stratigr. 45, 171–188.

Gröcke, D.R., Hesselbo, S.P., Jenkyns, H.C., 1999. Carbon-isotope composition of lower cretaceous fossil wood: ocean-atmosphere chemistry and relation to sea-level change. Geology 27, 155–158.

Hilbrecht, H., Frieg, C., Tröger, K.-A., Voigt, S., Voigt, T., 1996. Shallow water facies during the Cenomanian–Turonian anoxic event: bio-events, isotopes, and sea level in southern Germany. Cretac. Res. 17, 229–253.

Jarvis, I., Carson, G.A., Hart, M.B., Leary, P.N., Tocher, B.A., 1988. The Cenomanian–Turonian (Late Cretaceous) anoxic event in SW England: evidence from Hooken Cliffs near Beer, SE Devon. Newsl. Stratigr. 18, 147–164.

Jarvis, I., Gale, A.S., Jenkyns, H.C., Pearce, M.A., 2006. Secular variation in Late Cretaceous carbon isotopes and sea-level change: evidence from a new d13C carbonate reference curve for the Cenomanian–Campanian (99.6–70.6 Ma). Geol. Mag. 143, 561–608.

Jarvis, I., Lignum, J.S., Gröcke, D.R., Jenkyns, H.C., Pearce, M.A., 2011. Black shale deposition, atmospheric CO_2 drawdown, and cooling during the Cenomanian–Turonian oceanic anoxic event. Palaeoceanography 26 (PA3201), 1–17.

Jenkyns, H.C., 1980. Cretaceous anoxic events: from continents to oceans. J. Geol. Soc., Lond. 137, 171–188.

Jenkyns, H.C., 2010. Geochemistry of oceanic anoxic events. Geochem. Geophys. Geosyst. 11, Q03004. http://dx.doi.org/10.1029/2009GC002788.

Kuss, J., Scheibner, C., Gietl, R., 2000. Carbonate platform to basin transition along an Upper Cretaceous to Lower Tertiary Syrian Arc Uplift, Galala Plateaus, Eastern Desert, Egypt. GeoArabia 5, 405–424.

Lüning, S., Kolonic, S., Belhadj, E.M., Cota, L., Baric, G., Wagner, T., 2004. Integrated depositional model for the Cenomanian–Turonian organic-rich strata in North Africa. Earth-Sci. Rev. 64, 51–117.

Nagm, E., Wilmsen, M., 2012. Late Cenomanian–Turonian (Cretaceous) ammonites from Wadi Qena, central Eastern Desert, Egypt: taxonomy, biostratigraphy and palaeobiogeographic implications. Acta Geol. Pol. 62 (1), 63–89.

Nagm, E., Wilmsen, M., Aly, M., Hewaidy, A., 2010a. Cenomanian–Turonian (Cretaceous) ammonoids from the western Wadi Araba area, Eastern Desert, Egypt. Cretac. Res. 31, 473–499.

Nagm, E., Wilmsen, M., Aly, M., Hewaidy, A., 2010b. Biostratigraphy of the Upper Cenomanian–Turonian (lower Upper Cretaceous) successions of the western Wadi Araba, Eastern Desert, Egypt. Newsl. Stratigr. 44, 17–35.

Nagm, E., Wilmsen, M., Čech, S., Wood, C.J., 2011. An inoceramid bivalve tentatively assigned to the group of Inoceramus pictus from the Upper Cenomanian of Egypt (Galala Formation, Wadi Qena, central Eastern Desert). Freib. Forsch. C540, 91–102.

Nemoto, T., Hasegawa, T., 2011. Submillennial resolution carbon isotope stratigraphy across the oceanic anoxic event 2 horizon in the Tappu section, Hokkaido, Japan. Palaeogeogr. Palaeoclimatol. Palaeoecol. 309, 271–280.

Paul, C.R.C., Lamolda, M.A., Mitchell, S.F., Vaziri, M.R., Gorostidi, A., Marshall, J.D., 1999. The Cenomanian–Turonian boundary at Eastbourne (Sussex, UK): a proposed European reference section. Palaeogeogr. Palaeoclimatol. Palaeoecol. 150, 83–121.

Philip, J., Floquet, M., 2000. Late Cenomanian (94.7–93.5). In: Dercourt, J., Gaetani, M., Vrielynck, B., Barrier, E., Biju-Duval, B., Brunet, M.F., Cadet, J.P., Crasquin, S., Sandulescu, M. (Eds.), Atlas Peri-Tethys Palaeogeographical Maps. CCGM/CGMW, Paris, pp. 129–136.

Richardt, N., Wilmsen, M., 2012. Lower Upper Cretaceous standard section of the southern Münsterland (NW Germany): carbon stable-isotopes and sequence stratigraphy. Newsl. Stratigr. 45 (1), 1–24.

Rosenthal, E., Weinberger, G., Almogi-Labin, A., Flexer, A., 2000. Late Cretaceous-Early Tertiary development of depositional basins in Samaria as a reflection of eastern Mediterranean tectonic evolution. Am. Assoc. Pet. Geol. Bull. 84, 997–1114.

Sageman, B.B., Meyers, S.R., Arthur, M.A., 2006. Orbital time scale and new C-isotop record for Cenomanian–Turonian boundary stratotype. Geology 34, 125–128.

Said, R., 1990. The Geology of Egypt. Rotterdam (Balkema). 721p.

Schlanger, S.O., Jenkyns, H.C., 1976. Cretaceous oceanic anoxic events: causes and consequences. Neth. J. Geosci. 55, 179–184.

Schlanger, S.O., Arthur, M.A., Jenkyns, H.C., Scholle, P.A., 1987. The Cenomanian–Turonian oceanic anoxic event I. Stratigraphy and distribution of organic carbon-rich beds and the marine dC excursion. In: Brooks, J., Fleet, A.J. (Eds.), Marine Petroleum Source Rocks. Geological Society of London Special Publication, vol. 26, pp. 371–399.

Sharland, P.R., Archer, R., Casey, D.M., Davies, R.B., Hall, S.H., Heward, A.P., Horbury, A.D., Simmons, M.D., 2001. Arabian Plate sequence stratigraphy. GeoArabia, Spec. Publ. 2, 1–371.

Takashima, R., Nishi, H., Huber, B.T., Leckie, R.M., 2006. Greenhouse world and the Mesozoic ocean. Oceanography 19 (4), 82–92.

Tsikos, H., Jenkyns, H.C., Walsworth-Bell, B., Petrizzo, M.R., Forster, A., Kolonic, S., Erba, E., Premoli Silva, I., Baas, M., Wagner, T., Sinninghe Damsté, J.S., 2004.

Carbon isotope stratigraphy recorded by the Cenomanian–Turonian oceanic anoxic event: correlation and implications based on three key localities. J. Geol. Soc. Lond. 161, 711–719.

Van Bentum, E.C., Hetzel, A., Brumsack, H.J., Forster, A., Reichart, G.J., Sinninghe Damsté, J.S., 2009. Reconstruction of water column anoxia in the equatorial Atlantic during the Cenomanian–Turonian oceanic anoxic event using biomarker and trace metal proxies. Palaeogeogr. Palaeoclimatol. Palaeoecol. 280, 489–498.

Van Buchem, F.S.P., Razin, P., Homewood, P.W., Heiko Oterdom, W., Philip, J., 2002. Stratigraphic organization of carbonate ramps and organic-rich intraself: Natih formation (middle Cretaceous) of northern Oman. Am. Assoc. Pet. Geol. Bull. 86, 21–53.

Voigt, S., Gale, A.S., Voigt, T., 2006. Sea-level changes, carbon cycling and palaeoclimate during the Late Cenomanian of northwest Europe; an integrated palaeoenvironmental analysis. Cretac. Res. 27, 836–858.

Voigt, S., Aurag, A., Leis, F., Kaplan, U., 2007. Late Cenomanian to Middle Turonian high-resolution carbon isotope stratigraphy: new data from the Münsterland Cretaceous Basin, Germany. Earth Planet. Sci. Lett. 253, 196–210.

Voigt, S., Erbacher, J., Mutterlose, J., Weiss, W., Westerhold, T., Wiese, F., Wilmsen, M., Wonik, T., 2008. The Cenomanian–Turonian of the Wunstorf section (North Germany): global stratigraphic reference section and new orbital time scale for oceanic anoxic event 2. Newsl. Stratigr. 43, 65–89.

Wendler, I., 2013. A critical evaluation of carbon isotope stratigraphy and biostratigraphic implications for Late Cretaceous global correlation. Earth-Sci. Rev. 126, 116–146.

Wendler, J.E., Lehmann, J., Kuss, J., 2010. Orbital time scale, intra-platform basin correlation, carbon isotope stratigraphy and sea-level history of the Cenomanian–Turonian Eastern Levant platform, Jordan. Geol. Soc., Lond., Spec. Publ. 341, 171–186.

Wendler, I., Willems, H., Gräfe, K.-U., Ding, L., Luo, H., 2011. Upper Cretaceous inter-hemispheric correlation between the Southern Tethys and the Boreal: chemo- and biostratigraphy and paleoclimatic reconstructions from a new section in the Tethys Himalaya, S-Tibet. Newsl. Stratigr. 44, 137–171.

Wendler, J.E., Meyers, S.R., Wendler, I., Kuss, J., 2014. A million-year-scale astronomical control on Late Cretaceous sea-level. Newsl. Stratigr. 47 (1), 1–19.

Wilmsen, M., Nagm, E., 2013. Sequence stratigraphy of the lower Upper Cretaceous (Upper Cenomanian–Turonian) of the Eastern Desert, Egypt. Newsl. Stratigr. 46 (1), 23–46.

Wilmsen, M., Niebuhr, B., Chellouche, P., Pürner, T., Kling, M., 2010. Facies pattern and sea-level dynamics of the early Late Cretaceous transgression: a case study from the lower Danubian Cretaceous Group (Bavaria, southern Germany). Facies 56, 483–507.